

Chapter II.4

Superconductivity: introduction on RF vs. magnet

Claire Z. Antoine

Université Paris-Saclay, CEA, Département des Accélérateurs, de la Cryogénie et du Magnétisme, 91191, Gif-sur-Yvette, France

The aim of this lecture is to provide to physicists non-expert in material science a glimpse on how materials are tailored (and must be chosen) for their specific applications in accelerators. After an introduction the lecture is divided in three parts: 1) Recall on superconductivity: how and when to use the various models, 2) Vortex behavior: how it fixes the limits of operation in a superconductor, 3) Optimization of superconducting materials according to their applications.

II.4.1 Introduction

For decades, copper has been used for both acceleration and deviation, to fabricate electromagnets for curvature and focalization of the beam or RF cavities for acceleration. It is possible to replace copper by a superconductor (SC), but then, the specifications of the superconductors differ wherever magnetic field or electric field generation is concerned¹.

II.4.1.1 Superconductors in accelerators: why?

They are two main application of superconductivity in accelerators: electromagnets for beam deviation (curvature, focalization) and accelerating RF cavities.

II.4.1.1.1 DC applications and electromagnets

In direct current (DC), in specific conditions, the resistance of a superconductor is strictly equal to 0. Superconductivity allows phenomenal savings in weight, volume and energy consumption. For instance, SC cables about 1 mm × 10 mm section, as shown in Fig. II.4.1, can drive ~ 15 000 A—where a copper cable would require a 10 cm × 10 cm section.

Magnetic field is also required in detectors to curve the trajectory of charged particles and help identifying them, but no detecting element can be placed at the location of the magnet. Here again, even with the presence of cumbersome cryostats, superconductors allow a better “transparency”, as SC magnets occupy roughly 1/3rd of the volume (and weight) of copper magnets.

This chapter should be cited as: Superconductivity: introduction on RF vs. magnets, C. Antoine, DOI: [10.23730/CYRSP-2024-003.1057](https://doi.org/10.23730/CYRSP-2024-003.1057), in: Proceedings of the Joint Universities Accelerator School (JUAS): Courses and exercises, E. Métral (ed.), CERN Yellow Reports: School Proceedings, CERN-2024-003, DOI: [10.23730/CYRSP-2024-003](https://doi.org/10.23730/CYRSP-2024-003), p. 1057.

© CERN, 2024. Published by CERN under the [Creative Commons Attribution 4.0 license](https://creativecommons.org/licenses/by/4.0/).

¹A more complete version of this lecture is available at <http://arxiv.org/abs/2310.09097>.

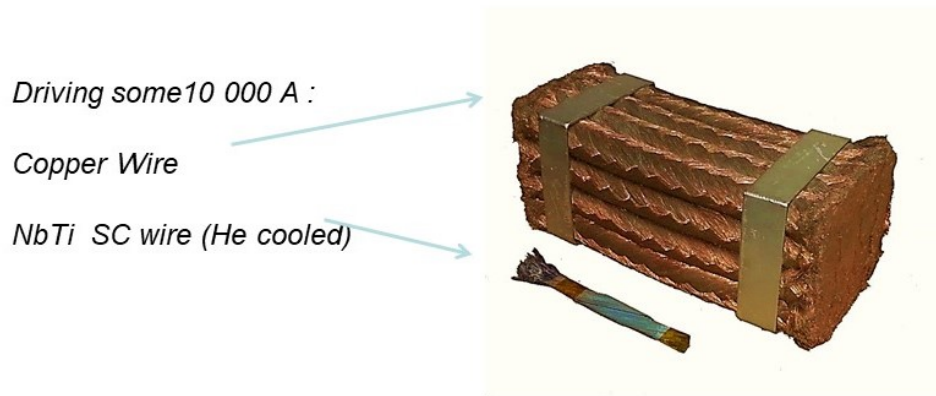


Fig. II.4.1: Required size for copper vs. superconducting cables (Courtesy of B. Hervieu).

II.4.1.1.2 RF cavities

For RF cavities, the situation is more complex, it depends a lot on the duty cycle. First of all the surface resistance is not null, but is about a factor 10^5 smaller than copper surface resistance in RF. Superconducting cavities exhibit very high quality factors at high duty cycle, but are limited around a few 10s of MV/m, the exact figure depending on the cavity geometry. Copper cavities can go to very high fields (some 100s of MV/m), but only with very low duty cycle. A duty cycle of 1 (beam power 100% of the time, also referred to as “continuous wave” (CW)) can only be reasonably achieved with superconductors. For copper cavities, power dissipation is a huge constraint. Most of the power transforms into heat instead of increasing beam energy, hence, cavity design is driven by this fact. Small duty cycle often imply higher frequencies operation to compensate the decrease integrated intensity.

For SC cavities, power dissipation is minimal, the cavity design can be decoupled from the dynamic losses and one gains the freedom to adapt design to specific applications, and lower frequencies are available. From the design point of view, the cavities openings are larger and the impedance is lower, which leads to reduced wake field and better emittance. In addition, alignment is easier. Unfortunately one loses on the cryogenic efficiency. Therefore, although Q_0 are $\sim 10^5$ higher than for copper, the plug power gain is only between 2 and 500 times better with SC dependent on the applications. Even if reducing costs by a factor of 2 is desirable—when dealing with research accelerators where a cryogenic plant cost several 10s M€—the annual cryogenic power consumption is also several 10s M€ for its ~ 30 years of existence. In fact, it is not always desirable to use superconducting cavities. Figure II.4.2 represents a coarse cost estimation in an arbitrary unit. Only the area covered by the blue ellipsoid present some advantages in using superconductivity.

II.4.2 Superconductivity

Superconductivity is a physical phenomenon discovered in 1911, but is still not fully described by a general theory up today. In the following, we will describe the general features for conventional superconductors (low T_C). The basic description requires using thermodynamic notions on phase transition. For those not familiar with this approach, see the extended version or textbooks.

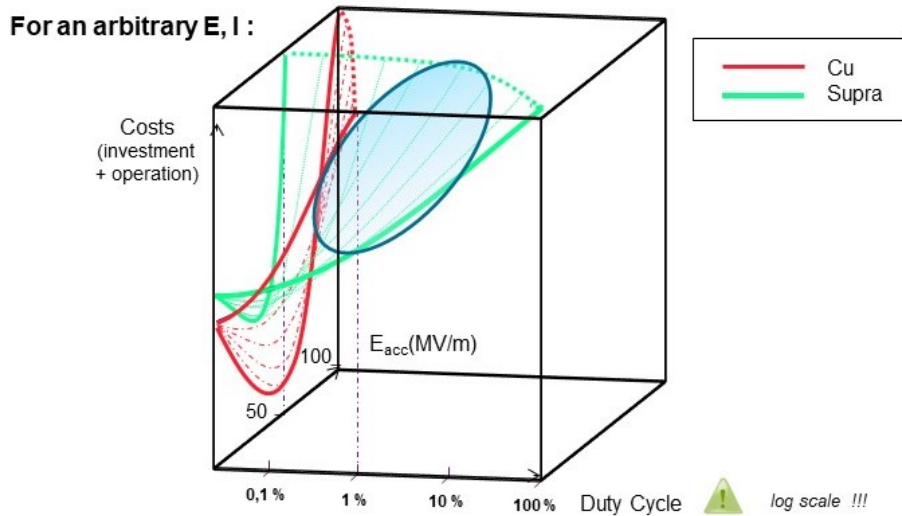


Fig. II.4.2: Coarse estimation of costs for a superconducting vs. copper accelerator. The blue ellipsoid show the domain of application where superconductivity is preferable.

II.4.2.1 Main features

II.4.2.1.1 Meissner state in presence of magnetic field

Superconductivity appears below a critical temperature T_C . More generally, when a superconductor is held at low temperature, low current density and is submitted to an external magnetic field, supercurrents develop at its surface (over a few 10s nm) and generate an opposite magnetic moment so that inside the material one gets:

$$\vec{B} = \mu_0(\vec{H} + \vec{M}) = 0 \quad . \quad (\text{II.4.1})$$

All magnetic field lines are expelled from the superconductor. This state is called “Meissner state”, and is common to all superconductors. The depth over which the field is damped is called λ_L , the penetration depth and will be detailed in Section II.4.2.1.4.

II.4.2.1.2 Type-I and type-II superconductors

For type-I superconductors, when the magnetic field exceeds a critical value (H_C), the material becomes normal conducting. H_C is the thermodynamic transition field for type-I SC. Type-II SC have a different behavior: they are in the Meissner state until the field reaches the first critical field, H_{C1} . Then some flux lines start to enter the material, forming a vortex (see Fig. II.4.3). A vortex is a single flux line (a quantum of flux) in a normal zone surrounded by screening currents.

Around the vortices², the superconductivity persists until the field reaches the second critical field (H_{C2}), where the material finally becomes normal conducting. The phase between H_{C1} and H_{C2} is called the mixed state or the vortex state (see Fig. II.4.3 and II.4.5, b). In the mixed state, the external field is not fully screened anymore. This can be verified by magnetometry, by measuring the magnetic moments

²One vortex in singular, several vortices in plural!

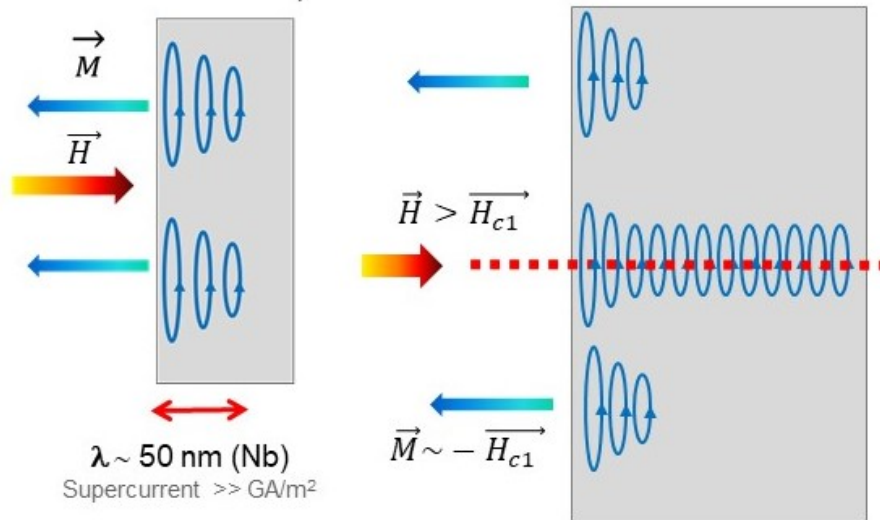


Fig. II.4.3: Meissner state (full field expulsion, left) and mixed state (mixture of normal and superconducting regions, right).

of superconducting samples as depicted in Fig. II.4.4. Contrary to H_C , H_{C1} and H_{C2} are not intrinsic thermodynamic figures, but depend on the purity and the mechanical state of the SC. Among the several 10 000s identified superconductors [1], only a dozen superconductors led to effective applications.

In accelerators, for now, only conventional materials (metals or alloys) are in use. They all exhibit a low H_{C1} and a high H_{C2} , and they operate in the mixed state, except Nb for RF applications. Indeed, if one puts a vortex in an oscillating field, it would start to move, along with its normal conducting core, and it would give rise to resistive thermal dissipation. That is why RF application are not based on the same material as magnet application. Up to today, only Niobium, the SC material with the highest known H_{C1} , has good performances in RF. This will be further detailed in Section II.4.4. Figure II.4.5, a) represents the SC phase diagram for type-II superconductors in the 3D (T, H, J) space. T_C , H_C , H_{C1} , and H_{C2} , have already been introduced. On this graph, one can observe also two other parameters: J_C and J_D . J_C , the so-called “critical current” is in fact a technical limit devised by the magnet community and has no thermodynamic/physical meaning outside its field of application (it will be discussed in Section II.4.3.3.2). J_D , the depairing current is in fact the thermodynamic “critical” value: when the current density reaches this value, it is high enough to break the Cooper pairs.

II.4.2.1.3 Vortex and flux quantization, penetration depth, coherence length, superconducting gap

In a defect-less material, each vortex contains one quantum of flux $\phi_0 = h/(2e) = 2,06783376 \times 10^{-15}$ Weber (or Tesla/m²); h is the Planck constant, e is the electron charge. The screening currents decrease over λ , the penetration depth, while the radius of the normal conducting zone is ξ , also called Cooper pair coherence length. λ and ξ are critical parameters that characterize each superconductors; they depend on its purity and mechanical state, and they diverge close to T_C . Note that the parameter κ introduced in Fig. II.4.4 is called the Ginzburg-Landau parameter and is equal to λ/ξ . It also depends on

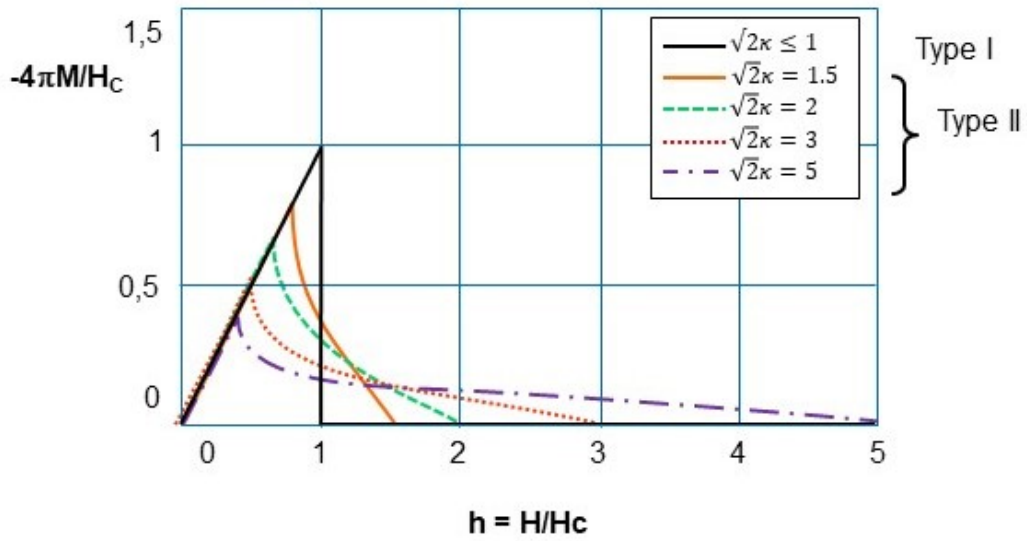


Fig. II.4.4: Reduced magnetic moment of different types of defect-free superconductors. κ is a figure of merit for a given superconductor and will be described below.

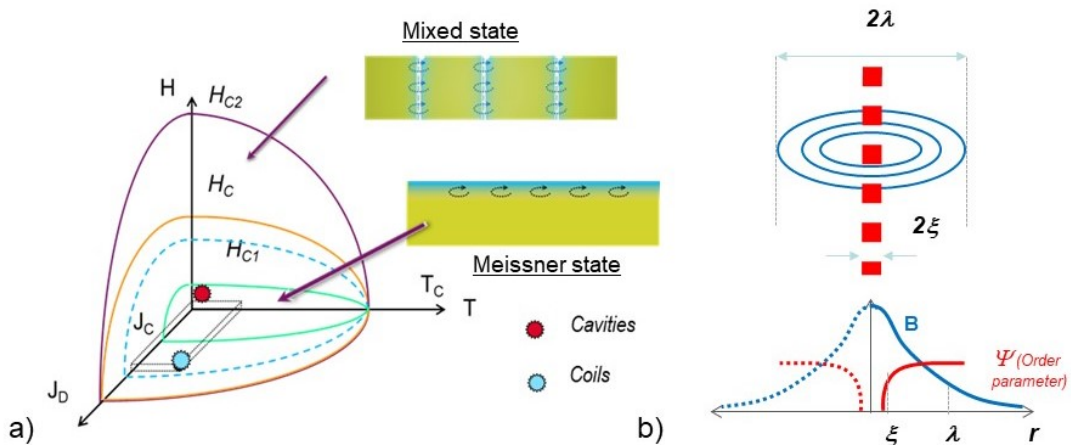


Fig. II.4.5: a) Phase diagram of type-II superconductors in temperature, magnetic field and current density. The red star indicates the operation range of SC cavities and the blue star indicates the range of operation of SC electromagnets. b) Details on vortex structure.

the material state, but is T independent. One can also define an order parameter ψ , which is equal to 0 in the normal state and reaches positive values in the superconducting state (see Fig. II.4.5 b). Vortices behavior is what conditions all applications (see Section II.4.3). Another parameter that characterizes a superconductor is the superconducting gap Δ : at the transition, an absorption band appears around $10^{11} - 10^{12}$ Hz ($\sim 10^{-3} - 10^{-4}$ eV, \sim some K) which indicates the opening of the superconducting gap, which is related to T_C^3 .

³See extended version <http://arxiv.org/abs/2310.09097> for details.

II.4.2.1.4 Ginzburg-Landau parameter and applications

Figure II.4.6 presents another type of phase diagram: the reduced field H/H_C as a function of the Ginzburg-Landau parameter κ .

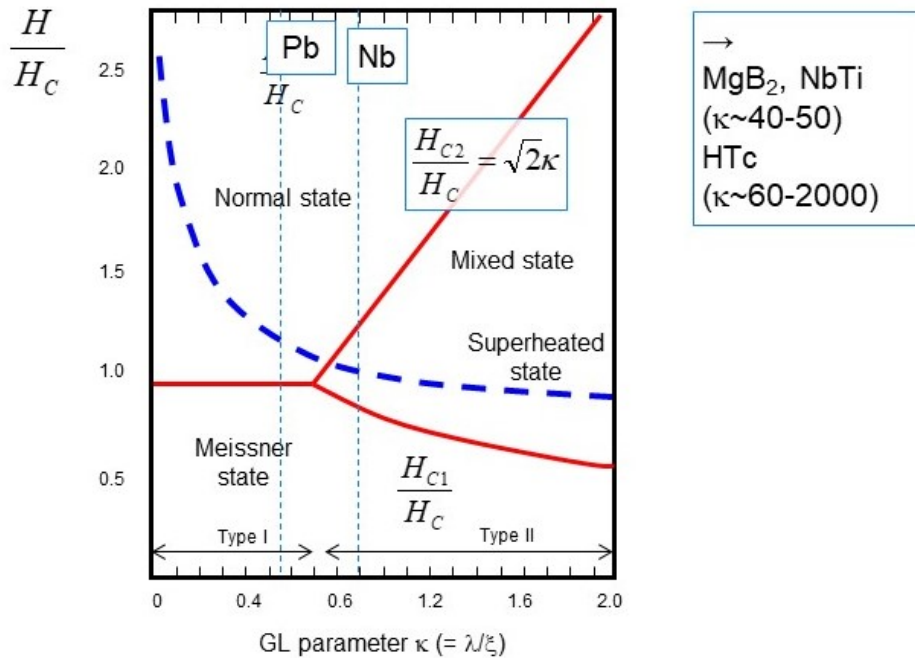


Fig. II.4.6: Reduced field H/H_C vs. the Ginzburg-Landau parameter κ . Superconductors with $\kappa > 1/\sqrt{2}$ are all type-II. Nb is very close to the type-I/type-II frontier, and therefore exhibit a very high H_{C1} . Blue dotted line figures superheating field, where Meissner state can be observed above its thermodynamic limits, as a metastable state.

It allows a better understanding of the difference between type-I and type-II SC. One can observe that most of the practical SC have a high κ except Nb that is very close to the type-I/type-II frontier. The dotted blue curve shows in addition the existence of a “superheating field” H_{SH} . H_{SH} is a metastable⁴ field below which Meissner state can be observed above H_C (type-I) or H_{C1} (type-II). It is mentioned here because it is believed that when the magnetic field is parallel to the surface, as is the case in RF cavities, this metastable state can be favored, and it is considered to be the ultimate limit in superconducting radiofrequency (SRF) cavities. This point will be discussed further in Sections II.4.3.2.2 and II.4.4.2.3.

II.4.2.1.5 The importance of the electronic mean free path ℓ

In Section II.4.2.1.3, we have mentioned that λ and ξ depend on the purity and mechanical state of the superconductor. In fact, modifying ℓ , one can tune the properties of the superconductor for a dedicated application, which is widely used for magnet wires. When ℓ decreases, ξ decreases while λ and κ increase, according to

⁴For example, very pure water can still be liquid (super cooled state) below 0°C. The slightest shock will make it become solid very quickly. See e.g. [Watch supercooled water freeze - YouTube](#). By definition, a metastable state is not very stable ...

$$\frac{1}{\xi} = \frac{1}{\xi_0} + \frac{1}{\ell} \quad , \quad (\text{II.4.2})$$

$$\lambda = \lambda_L \cdot \left(\frac{\xi_0}{\xi}\right)^{\frac{1}{2}} = \lambda_L \cdot \left(1 + \frac{\xi_0}{\ell}\right)^{\frac{1}{2}} \quad . \quad (\text{II.4.3})$$

λ_L is an estimation of λ for a "perfect SC" introduced by the 2-fluid model (see below). The size of a Cooper pair is also assimilated to ξ_0 (at $T = 0$) because it is a system coherence length, but do recall the ξ parameter was introduced in the GL model to account for the variation of the order parameter at the vortex core. Note that the size of a Cooper pair does not vary with T , only their density.

II.4.2.2 Superconductivity models

Superconductivity remained a puzzle for decades for lack of finding a theory that could face all the physical aspects observed during the transition from the normal to the superconducting state. In the literature, one can find many particular complex developments that apply to very specific conditions and have limited range of validity. The early advances in that domain have been mostly performed by the "magnet" community. Most of the development presented as general in classical lectures and textbook apply in fact only to a specific type of SC as will be seen in Section II.4.3, and cannot be extended directly to the case of high T_C (see Section II.4.4.1.4) or of niobium in use in RF. Actually, there is no complete theory for superconductivity yet, and it is important to keep in mind the condition in which a model can be used⁵. In the following, we will just describe the contour and limits of application of the most common models.

II.4.2.2.1 London: 2-fluid model (1935)

The 2-fluid model was proposed by Gorter and Casimir (1934) to explain superfluidity in Helium. Then F. and H. London used it to explain the Meissner effect. It is a phenomenological classic theory. It explains Meissner effect and defines λ_L that predicts λ within a factor 2. It works well if $J_S \ll J_D$ and n_s (superelectrons density) is uniform⁶. It is valid for any temperature T , but only at low B since at high B nonlinear behaviors appear. Predictions are not very accurate for thin films.

II.4.2.2.2 Ginzburg–Landau model (1950) and its extensions

The Ginzburg–Landau (GL) model is based on the combination of electromagnetism and thermodynamics, in particular second-order phase transitions. It introduces quantum aspects: one single wave function for all Cooper pairs, the coherence length ξ and the order parameter ψ is called "wave function of condensed electrons". This order parameter measures the symmetry breaking energy U needed for the superconducting state to appear. The condensation energy is $1/2\mu_{OH_{C2}}$. In the presence of H , n_s can vary, and the free energy can be written as a Taylor development in function of the order parameter ψ . Developing 1st or 2nd order is valid only near transition ($T \sim T_C$ or if $T \sim 0$ K, $H \sim H_{C2}$). The solution is found by minimizing ψ (the wave function) and A (the vector potential) over all space. It

⁵Detailed description of the models can be found in the extended version <http://arxiv.org/abs/2310.09097>, or in solid state physics textbooks.

⁶Not always true, see Section 3.

requires long and complex calculation that results into two coupled nonlinear differential equations that can be solved only numerically. Numerical predictions are similar to London, but the prediction of thin films behavior is better.

The **GLAC** (Ginzburg–Landau–Abrikosov–Gor’kov) model is an extension of GL that incorporates the effects of impurities and magnetic fields on superconductivity (“dirty” SC). It provides a better description of type-II superconductors. The **Linear GL** approach has been developed for high κ superconductors for magnet applications at low temperature but high field (close to H_{C2}). In this case, $\xi(T)$ and $\lambda(T)$ are very large since they diverge for $H \sim H_{C2}$. At ξ and λ scale one can assume that changes in ψ and Δ at a normal-superconducting interface are \sim linear. In short, in this case one can also neglect second-order in the Taylor expansion and GL equations becomes decoupled. This approach applies only for high κ SC and cannot be used for RF niobium.

Note: London and GL models rather apply to type-II superconductors. For type-I, the developments were proposed by Pippard.

II.4.2.2.3 BCS (Bardeen–Cooper–Schrieffer), (1957) and its extensions

BCS is the most complete theory. It is a local (microscopic), quantum theory. It explains the main aspects of SC (gap, T_C , critical parameters) and works at arbitrary ℓ , arbitrary T , arbitrary H . The Cooper pairs are electrons with opposed moments p and spins, there is one single wave function for each Cooper pairs, but the system is highly correlated with many exchanges between pairs. The total energy of the interacting pairs remains constant although their moments are constantly changing (quantic delocalization behavior: a cooper pair does not concern two determined individual electrons but two electrons with opposed moments and spins at each instant t). BCS theory is essentially used to make exact calculation and comfort GL hypothesis (same results at $T \sim T_C$). In general, it is not used for engineering predictions (too complex). Compared to GL model, BCS introduces the role of phonons, the existence Cooper pairs, and the BCS gap (slightly different from the one calculated in G.L). The e^- /phonon interaction is described with an effective potential and the use of second order perturbation theory. In fact, BCS is not a complete theory; it works mainly for low coupling systems (high κ type-II). High coupling systems like Nb and type-I need corrections.

If there is a strong interaction between pairs, one can no longer make a perturbative treatment, it is necessary to make a variational approach. The Eliashberg model directly takes into account strong e^- /phonon coupling. Several other specific developments have been made, for instance: Bogolubov–De Gennes (1965): concerns arbitrary ℓ , arbitrary T , arbitrary H , weak coupling electron-phonon, and the order parameter depends on position; Eilenberger (1968): arbitrary ℓ , arbitrary T , arbitrary H , type-II semi-classical theory, applies to “clean” type-II SC; takes into account some inhomogeneity, but not valid at low T ; Usadel (1970): extension of Eilengerber with dirty limit approximation: $\ell \leq \xi$.

II.4.2.2.4 Radiofrequency

Response to EM wave has been treated by Mattis–Bardeen in 1958 at weak field, in the Pippard ($\xi \gg \lambda$) approximation, and using the 2-fluid approach ($\sigma = \sigma_n + i\sigma_s$) [2]. The equations are used for type-II nonetheless. At high current density ($J \sim J_D$), “non linear R_{BCS} ” model has been developed by

Gurevich in 2006, only for clean type-II SC [3]. At low and medium field one can derive the following equation for RF surface resistance:

$$R_{\text{BCS}} = A(\lambda_L^4, \xi_F, \ell\sqrt{\rho_n}) \frac{\omega^2}{T} e^{-\Delta/kT} \quad . \quad (\text{II.4.4})$$

Here A is a constant depending on λ_L (the penetration depth of the magnetic field), ξ (the coherence length of the Cooper pairs), ℓ (the mean free path of the quasi-particles) and ρ_n (conductivity in the normal state); ω is the angular RF frequency; Δ the superconducting gap and T the temperature. R_{BCS} is due to the scattering of the normal electrons of the superconductor over the lattice (issued from thermally activated broken Cooper pairs). Other pair breaking mechanisms are not included in this model).

II.4.3 Mixed state and applications

As stated before, the frontiers of mixed state is what conditions the applications of a superconductor, magnet or RF cavities. The needs are specifically different for both applications: for electromagnets one aims at very high current densities with 0 resistance (in DC). It implies that they are in the mixed state, with non-moving, trapped vortices, medium fields ($H_{C1} < H_{\text{operation}} < H_{\text{irr}}$, H_{irr} will be defined below). Defects are voluntarily introduced to enhance pinning. The effect is to decrease the mean free path ℓ and H_{C1} and to increase H_{C2} . Magnets operate below a critical current density J_C about 10–15% of the depairing current density J_D (see below).

For cavities, one aims at very high field with minimal dissipation but as showed in Section II.4.2.2.4, the surface resistance cannot be 0. Vortices cannot keep trapped at high frequency and submitted to a variable field, they would cause very high dissipation. So one has to prevent vortex entering in the material and work in the Meissner state. So one needs to reduce the number of defects that might promote early vortex penetration and use a material with very high H_{C1} and/or H_{SH} if accessible. In summary, superconductors fitted for magnet applications are bad for cavities applications—and vice-versa!

II.4.3.1 Vortices: penetration inside the superconductor

In this paragraph, we will describe the mechanism of vortex penetration and how some defects can promote early penetration.

If one considers an interface between a superconductor and a normal conducting region (or vacuum), to get the free energy, one has to balance the magnetic energy, where the induction B decreases over λ and the condensation energy where the density of superconducting electron grows over ξ .

Figure II.4.7 shows the typical interface free energy for type-I and type-II superconductors at relatively high field ($H \sim 0.7 H_C$). One can observe that for type-II superconductors, the free energy is negative close to the surface. It means that it is energetically favorable to nucleate a normal zone at high field, leading to the generation of vortices.

Magnetic energy:

$$\delta g_m \sim \mu_0 \frac{H^2}{2} \left(1 - e^{-\frac{x}{\lambda_L}}\right) \quad , \quad (\text{II.4.5})$$

Condensation energy:

$$\delta g_{\text{cond}} \sim \mu_0 \frac{H_C^2}{2} \left(\frac{n(x)}{n_s}\right) \quad . \quad (\text{II.4.6})$$

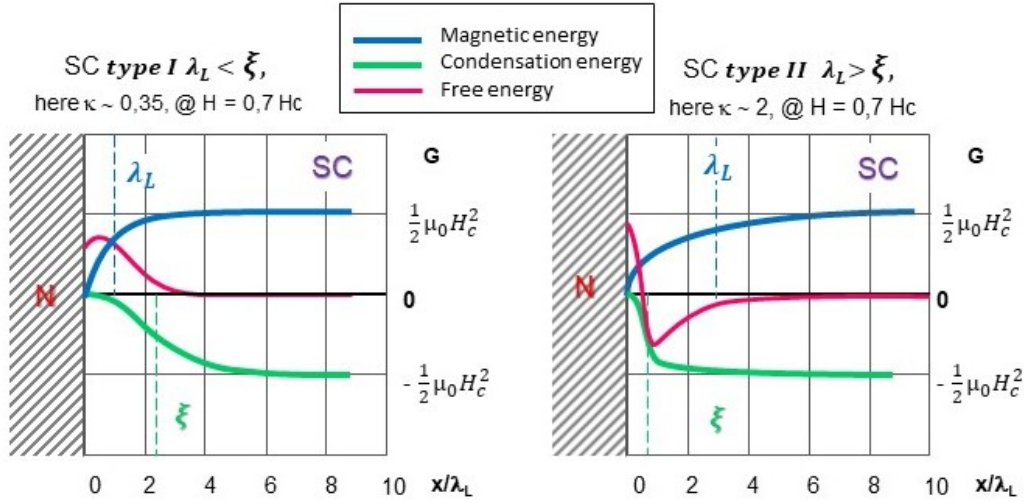


Fig. II.4.7: Variation of the magnetic energy and the condensation energy that compose the free energy. For type-II SC with $\lambda > \xi$, the free energy is negative, which means it is energetically favorable to create a NC/SC interface.

The minimization of free energy leads to several predictions:

- The normal zone must be as small as possible ($\phi \sim 2\xi$); this holds only for $\xi < \lambda$ i.e. type-II SC;
- The magnetic size of the system is $\sim 2\lambda$ (a vortex is a normal region with one single flux line inside and screening currents around);
- The number of vortices is the one that minimize $\Delta G/L$, it depends on applied H and sample dimension;
- Surface stabilizes the apparition of the SC mixed state, and nucleation always occurs at surface, vortices always emerge perpendicular to the surface (see Fig. II.4.8);
- Vortices repel each other (but attract antivortices). In absence of defect, they form a regular hexagonal centered lattice so-called Abrikosov lattice.

II.4.3.2 Parallel versus perpendicular field

II.4.3.2.1 Demagnetization effects

In perpendicular field, the field lines enter easily on thin samples due to demagnetization factor. If one exposes an ellipsoidal sample to uniform field, the field on surface is the same everywhere, whereas if it has an arbitrary shape one has to consider the local deformation of flux line (antenna effect), as shown in Fig. II.4.9. Equation II.4.1 becomes

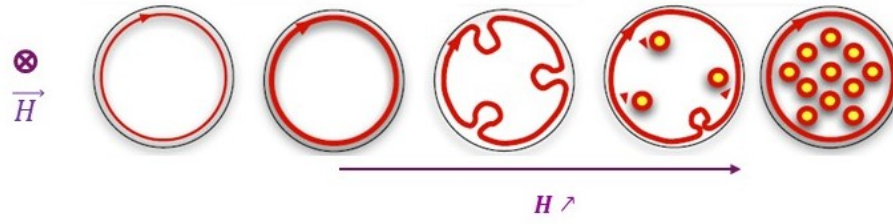


Fig. II.4.8: Schematic description of the vortices nucleation in a thin sample perpendicular to the magnetic field. In the Meissner state, current line flow (in red) around the sample according to Lorentz laws. As field increases, the current lines incurve to enclose a field line in the normal zone.

$$\vec{B} = \mu_0(\vec{H} + (1 - D)\vec{M}) = 0 \quad , \quad (\text{II.4.7})$$

where D is the demagnetization factor (for more details see Ref. [4]). At lower scale, roughness can also play a similar role. This effect makes it very difficult to measure accurately H_{C1} by classical magnetometry where the sample is immersed in a uniform field. It is a large source of discrepancies in the literature. Only the first penetration field can be measured, which is a convolution of H_{C1} and shape factors that can vary a lot with the preparation of the sample.

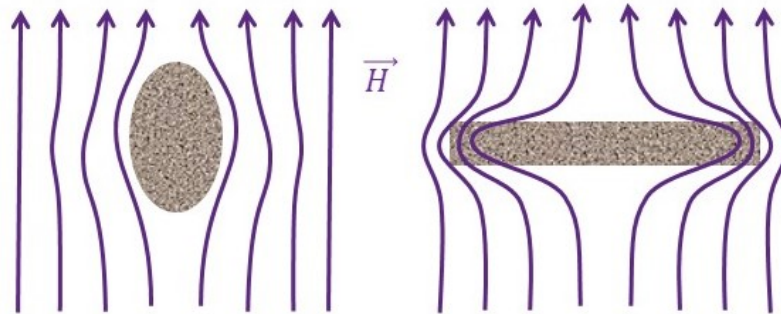


Fig. II.4.9: Effect of the edge of a thin slab sample on the deformation of the field line.

II.4.3.2.2 Surface barrier

In parallel field, the situation is different. One has to take into account the distortion of the potential introduced by the rupture of periodicity at the surface. This was formalized by Bean and Livingston in 1964 [5], by introducing an “image” vortex⁷ that allows to respect the $J_{\perp} = 0$ boundary condition. Therefore, before entering the material, vortices have to cross a surface barrier. The vortex thermodynamic potential can be expressed as

$$G(x) = \phi_0 [H_0 e^{-x/\lambda} - H_v(2x) + H_{C1} - H_0] \quad . \quad (\text{II.4.8})$$

⁷A similar approach exists in electrostatics with image electrons.

The first term in the bracket corresponds to Meissner induction decreasing at the surface, the second term corresponds to image vortex and $H_{C1} - H_0$ accounts for the fact that one must exceed H_{C1} to obtain stable vortices. Figure II.4.10 shows the modification of Eq.(II.4.8) when H_0 increases.

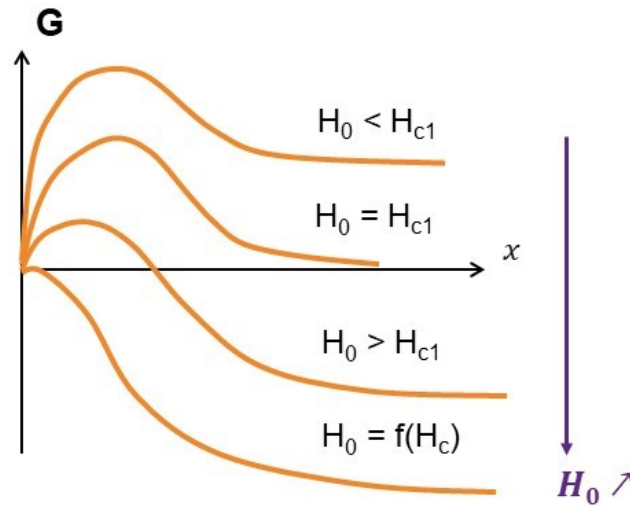


Fig. II.4.10: Vortex thermodynamic potential vs. depth for various applied field values.

When $H_0 \sim H_{C1}$, $G = 0$ in the depth of the material (vortices are stable), but there is still a barrier that prevents them to enter. On an “ideal surface”, the barrier disappears only at $H_{SH} \sim f(H_C) > H_{C1}$. So having parallel field stabilizes the superheating field, and that is the rationale used to predict SRF limits. Unfortunately, if there exist local defects, with for instance $H_C^{local} \ll H_C^{bulk}$ (or $T_C^{local} \ll T_C^{bulk}$), one can observe early penetration of several vortices there and the superheating state cannot be maintained. In this case, only material with a high H_{C1} can prevent vortex to enter. That is why niobium, with the highest H_{C1} of known superconductors has been a material of choice for SRF applications.

II.4.3.2.3 Morphologic defects

Realistic materials often exhibit morphologic defects: general shape, scratches, natural roughness, but also at smaller scale: crystalline facets, inclusions, atomic steps, etc. When parallel field encounters a morphologic defect, the magnetic field lines are compressed and the field is locally enhanced by a factor β . Even if the field enhancement on a defect is small, the first point reaching the transition field is obviously there. It is not the height of the steps that matters but the angle of curvature on the step edges [6]. Typically an etching pit often found after etching, with roughly a half-ellipsoid shape ($50 \mu\text{m} \times 100 \mu\text{m}$) has a β around 1.5–2. A crack in a thin film can go as high as a factor 5. In magnet, surface imperfections can be at the origin of flux trapping and flux jumps (see Section II.4.3.2.4). In SRF, roughness at the μm and the nm scale matters in the high magnetic field parts of the cavity: it can trigger an early quench. Note that similar features will also result in electric field enhancement on parts exposed

to high electric fields, but the consequences are not so drastic. The field enhancement required to draw electrons from the surface is one or two orders of magnitude higher. These two points will be further detailed in Section II.4.4.2.

II.4.3.2.4 Flux jumps and avalanche penetrations

Flux jumps are observed when a group of vortices is suddenly de-trapped, usually from the surface and start to enter the material⁸. It is a very common phenomenon observed in magnets when put under charge. If not well controlled it can become destructive. Indeed, if for some reason, the field or current or temperature is locally increased, vortices start to move, causing energy dissipation and a slight temperature rise. This temperature rise helps to detrap more vortices, which cause further dissipation and temperature rise. The phenomenon will rapidly lead to an avalanche penetration of vortices followed by such high dissipation that superconductivity is lost. For cavities, this point is of paramount importance. Typically, the period of a RF field is ~ 1 ns. It means that within a period, several hundred thousand vortices can enter the material in a $\sim 200 \mu$ and dissipate accordingly (see Fig. II.4.11). To be compared with $\lambda \sim 50$ to 250 nm for typical superconductors. This type of incident severely limits the use of a SRF cavity, and extra care must be taken to prevent the existence of surface defects that could promote early penetration.

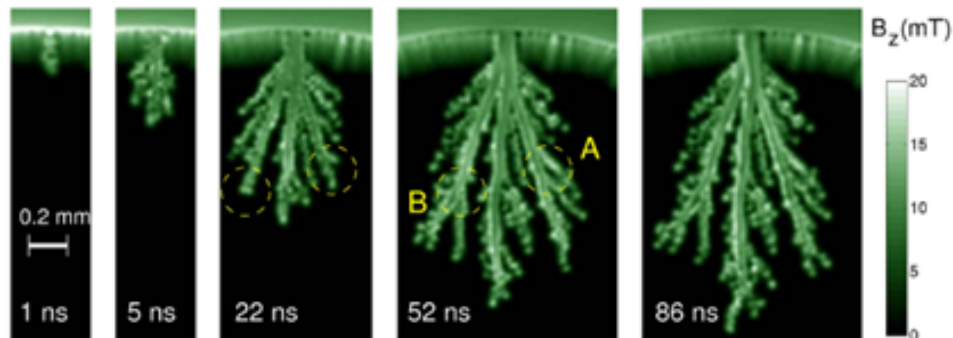


Fig. II.4.11: Magneto-optics view of avalanche penetration of vortices in MgB_2 at $T = 5$ K. One can observe that the phenomenon is fast: a few 100s nm deep within one ns, and that temperature and electric field reach high values. The complete burst corresponds to the entrance of several millions of vortices. Reproduced with the kind authorization from J. I. Vestgård (University of Oslo). For more details and movies, see Ref. [7].

II.4.3.3 Vortices in the presence of current

II.4.3.3.1 Flux flow resistance

In a perfect material, in the presence of current, vortices are submitted to the Lorentz force $\vec{F} = \vec{j} \times \vec{B}$, and start to move collectively at a constant speed v . It generates an electrical field $\vec{E} = -v \times \vec{B}$,

⁸RF applications, but also SC electronics, detectors. . .

parallel to \vec{j} . Because of Ohm law, if there is a potential difference, then the resistance cannot be 0 (see Fig. II.4.12). Indeed, one observes experimentally a non-negligible resistivity called “flux flow resistivity” ρ_{ff} . The movement of the vortices is limited by a viscous force (Magnus force), which originates from the normal zone dissipation. It is easy to determine that ρ_{ff} is proportional to $\rho_n \frac{B}{B_{C2}}$, since only a fraction of the surface is normal conducting and it depends on the number of vortices. When B reaches B_{C2} , the vortices overlap and the surface becomes completely normal conducting. The viscosity η equals $\phi_0 \frac{B}{B_{C2}}$ and the constant speed v equals $\frac{E}{B}$. The elastic energy of the system tends to keep the vortices equidistant.

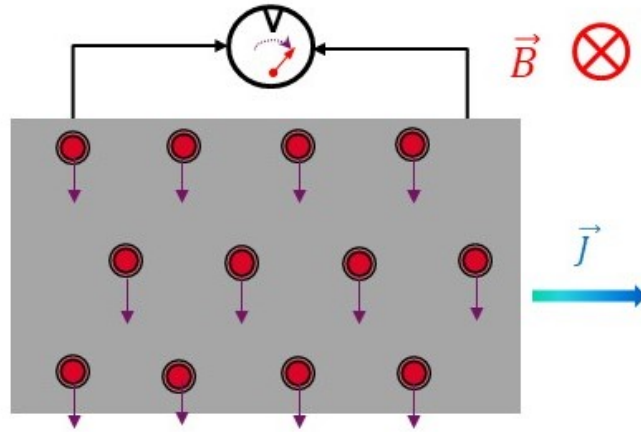


Fig. II.4.12: Movement of vortices in the presence of magnetic field and current density

Therefore, a perfect material in the mixed state the DC under field would never exhibit a resistance equal to 0 because of the movement of the vortices. Fortunately, actual materials always exhibit defects, especially if their composition is complex, and the first experimentalists obtained 0-resistance below a certain current density J_C , without knowing anything about pinning mechanism.

II.4.3.3.2 Critical current density J_C

In practice the resistance $R = 0$ in DC, only for $J < J_C$ for type-II SC in the mixed state, when vortices are pinned on pinning centers. At a certain point, the Lorentz forces overcome the pinning forces F_P and the vortices start to move again, reinstating the flux-flow resistance (see Fig. II.4.13). J_C is the current density at which flux-flow starts. F_P and therefore J_C depend on the temperature T and on the field B .

The projection of J_C in the H vs. T plane corresponds to H_M (“melting”), as the individual vortices move “liquid-like” beyond this field. It is equivalent to H_{irr} (“irreversible”) as measured in DC magnetometry. To increase J_C , one has to keep the vortices trapped, so one artificially incorporates defects (inclusions, grooves, alloying, damaging, etc.) as will be detailed in Section II.4.3.4. The electrons mean free path ℓ is reduced, which in turn decreases ξ and H_{C1} , and increases λ , κ and H_{C2} . Meissner state is marginal in these kinds of type-II SC, they transit readily into the mixed state. J_C is a technical limit defined for magnet purposes, J_C (extrinsic) $\ll J_D$ (intrinsic). It has no signification in RF where pinning is inefficient. Note that in low frequency AC regime, even if vortices are well pinned, they

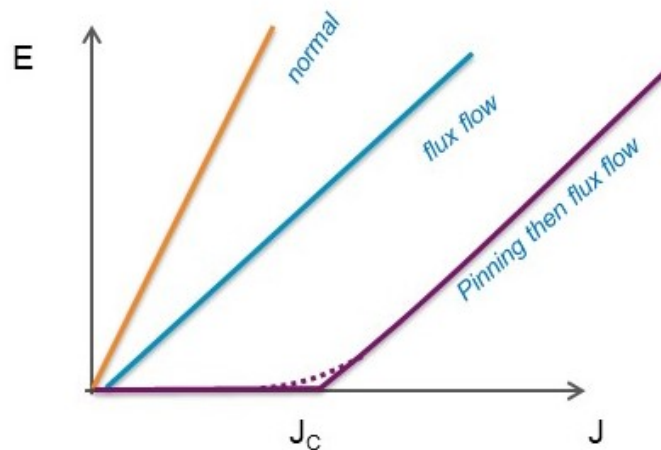


Fig. II.4.13: Electric field E vs. current density J . The slope of the curve is the resistance. Flux flow resistance is only a fraction of the normal conducting resistance, and in case of pinning, the apparition of non-0 resistance is delayed. Close to J_C one can observe some flux creep or flux jumps, before the collective movement starts.

oscillate in the pinning well and the resistance is never strictly equals to 0.

II.4.3.4 Pinning on crystalline defects

II.4.3.4.1 Crystalline defects at the atomic level

Figure II.4.14 gives some recalls on crystalline defects and their dimensionality. Dimensionality influences the distortion of the crystalline lattice and plays a large role in the local modifications of superconductivity. Any well-recrystallized material still contain an equilibrium concentration of each type of defects, which depends only on the temperature and purity.

Note: the elastic strain due to defects also plays a strong role in impurity segregation. For instance, H tends to gather around dislocation cores to form so-called “Cottrell clouds”. In Nb, one also observe H, and also C and O segregation at the oxide-metal interface, as shown in Ref. [6].

II.4.3.4.2 Simplified view or “saving condensation energy”

If normal conducting regions already exist, it is more favorable for a vortex to bend to go through this normal area because it saves condensation energy (remember that it requires a lot of energy to break one single Cooper pair). At the equilibrium, the cost in elastic energy (one has to bend the vortex) compensates the gain in condensation energy, as illustrated by Fig. II.4.15.

It is intuitive to understand that the resulting pinning force depends on the diameter d of the defect: for very small defect, the gain in condensation energy is minimum, while if the defect is much larger than the vortex core, the vortex becomes a simple flux line inside a normal conducting material.

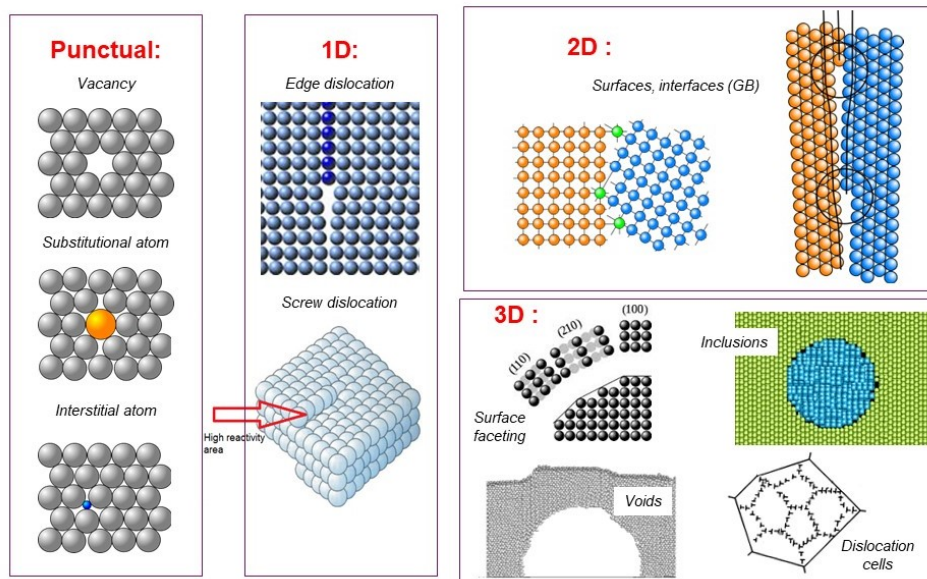


Fig. II.4.14: Examples of crystalline defects. Interfaces (e.g. grain boundaries) can be considered as an array of 1D defects for some orientations. Seemingly, a crystal is often subdivided into sub-crystals with slightly different orientations, separated by dislocation walls. Inclusions or voids are often encountered in industrially produced materials. Surfaces tends to reconstruct to exhibit crystalline planes with lesser energy. Even 1D defects tend to gather to form larger dimension defects.

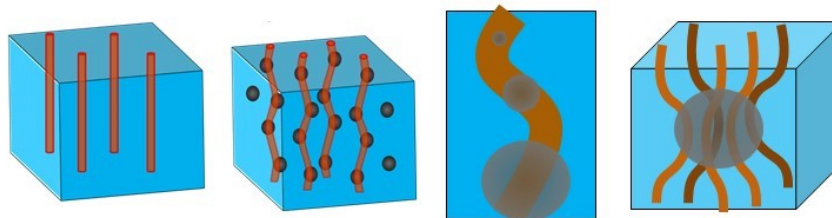


Fig. II.4.15: Left: without defects vortices are regularly spaced (Abrikosov Lattice). Right: effect of the size of normal conducting inclusions on the deformation of vortices. See text for details.

II.4.3.4.3 The four actual components of pinning

In his comprehensive book on flux pinning in superconductors [8], Matsushita describes four mechanisms:

- **A) Condensation energy variation:** one saves condensation energy if a normal zone already exists close by.
- **B) Elastic interactions:** there are several aspects:
 - Bending a vortex requires elastic energy,
 - The lattice elastic moduli in SC state smaller than the elastic moduli in the normal state [9],
 - The elastic deformation due to the presence of crystalline defects interacts with the local

elastic energy. The higher the dimensionality of the defect, the higher its influence on SC properties.

- **C) Magnetic interaction:** if a defects has dimension $\gg \lambda$, you can treat it like an N-S interface, with image vortex approach, the apparition of a surface barrier, etc. It is a very strong effect.
- **D) Kinetic energy interaction:** it concerns areas with different ξ and vortex velocities, and concerns very particular materials. It will not be detailed here.

What is important is that all these mechanism concern **local effects**, where the material exhibit non uniform properties. If one recalls Section II.4.3.2, models like the two-fluid model on the other hand apply for a uniform density of Cooper pairs. Similarly, the Ginzburg–Landau approach concerns slowly varying potential (see Section II.4.3.2.4). In the presence of pinning, classical models need to be revised to produce accurate prediction.

II.4.3.4.3.1 *Surface magnetic pinning vs. volume core pinning*

There are two ways to produce efficient pinning:

- “Surface magnetic pinning”: one needs a few strong pinning centers: twinning planes, voids, non-SC aggregates, irradiation defects (columnar), nano-indentations. In that case, the dominant mechanism is A then C then D. If the defect is large enough several vortices can get pinned on the same defect.
- “Volume core pinning” can be achieved with numerous weak pinning centers. In that case, the dominant mechanism is B. B is less efficient than C but if they are many pinning centers, it also results into strong pinning. As said previously, the efficiency of the B mechanism increases from 0-D (e.g. interstitial atom) defect to 3D defects (e.g. small inclusions). Large 3D defects with dimension $\gg \lambda$ fall under “surface magnetic pinning”.

II.4.3.4.3.2 *2D- Grain boundaries*

Grain boundaries (GB) are often presented as a typical efficient pinning center by most lecture on superconductivity, but in fact, it once again depends on applications. GBs constitute a loss of the crystalline order over n atomic distances; n depending on the crystalline structure and particular grain orientations. In a superconductor like bulk Nb, $n \sim 2 - 3$, so the disordered area is no larger than ~ 1 nm. Compared to the coherence length of Cooper pairs $\xi^{\text{Nb}} \sim 40$ nm, one can see that GB in Nb cannot play a strong role in pinning. Indeed, in Nb, dislocation cells which size is ~ 100 nm (so the same order of magnitude as $2\xi^{\text{Nb}}$) constitute a far more efficient pinning source [10]. In Nb thin films, on the contrary, grains are very small (~ 100 nm diameter) and the mean free path is much lower. The coherence length decreases accordingly (see Eq. (II.4.2), Section II.4.2.1.5), and GBs become effective pinning centers. For the HTC, YBCO family, n can reach up to 10 in some directions, (~ 3 nm) which is the same order of magnitude of ξ^{AB} (in the AB crystalline plane). In that case, the risk that a Cooper pair is scattered by the GB is very high, and GB constitute de facto very efficient pinning centers. Most of the SC used for magnets applications have usually a small ξ and fall under this situation.

II.4.3.4.4 Pinning at high frequency

Complex impedance measurement on SC samples allows determining the behavior of complex penetration depth $\lambda_{AC} = \lambda' + i\lambda''$ vs. frequency, as shown in Fig. II.4.16. The measured flux is $\phi_{AC} = \int b_{AC} dS \sim 2\lambda_{AC} \ell_b b_0$. At low frequency, when vortices are trapped, $\lambda' \sim \delta_{AC}$ (normal conducting penetration depth), whereas at high frequency, when the vortices cannot be kept pinned, $\lambda' \sim \lambda'' \sim \lambda_L \ll \delta_{AC}$. AC techniques are widely used to determine SC properties of cable material (surface susceptibility, surface impedance or surface resistivity) [8, 11]. In particular, susceptibility curves look a lot like the one shown in Fig. II.4.16 (in absolute value) vs. frequency or temperature. Increasing ω or T is equivalent to providing energy to free vortices from their pinning center.

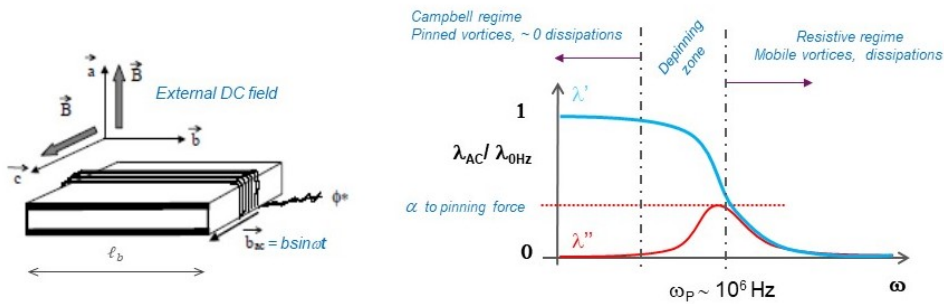


Fig. II.4.16: Complex penetration depth vs. frequency. At low frequency vortices (V_x) are pinned and the resistance is 0 (so-called Campbell regime), while at high frequency they move freely and the regime is resistive. The frequency where λ'' is maximum is called the “depinning frequency”. It can also be used to evaluate the pinning force. Picture from A. Pautrat (ENSICAEN), modified with permission.

This behavior is the reason why RF cavities must operate in the Meissner state: at radiofrequency, most of the vortices cannot be kept trapped and oscillate with the RF field, issuing high dissipation.

II.4.3.5 Conclusion on pinning

II.4.3.5.1 SRF cavities

There is no pinning at high frequency but if they are pinning centers in the material, they can prevent flux lines from being properly expelled during cooldown. Those trapped flux lines become oscillating vortices within $\sim \lambda$ and can be at the origin of hotspots [12].

II.4.3.5.2 Magnets

Pinning efficiency drives the critical current density J_C (and $R = 0$ range of application). Whenever possible, pinning features are amplified (impurities, deformation, alloying, voids, inclusions, topological defects, etc.), which leads to a modification of the mean free path and a large increase of J_C .

Thus, superconductors good for magnets application are terrible in RF conditions—and vice-versa!

II.4.4 Optimization of superconducting materials

As we have seen previously, the optimization of a superconducting material depends a lot on its application: magnet vs. RF cavities. Magnet is a much more mature technology; most of the wires are available in commercial companies. Some optimization of the cables can be conducted corresponding to a particular project, but the laboratory work consists mostly into optimizing the design from the mechanical and safety point of view. Cavities technology is more recent. Ultrapure Nb based technology is now available in 1–2 supplier worldwide, but improvements of the technology as well as R&D on successor materials are still actively under development in SRF labs. In the following paragraphs, we will provide a short description of some common materials. For more details, one needs to go to more advanced literature.

II.4.4.1 Magnets

Figure II.4.17 shows some examples of cables developed for various applications. The structure of the cables is complex, since it has to ensure several functions in addition to resistance-less conductivity: mechanical load and/or thermal transfer, uniformity of current flow, reduction of demagnetization effects, etc. The full detail of cable design is beyond the scope of this lecture, we will just provide a few examples of the development approaches in the following paragraphs.

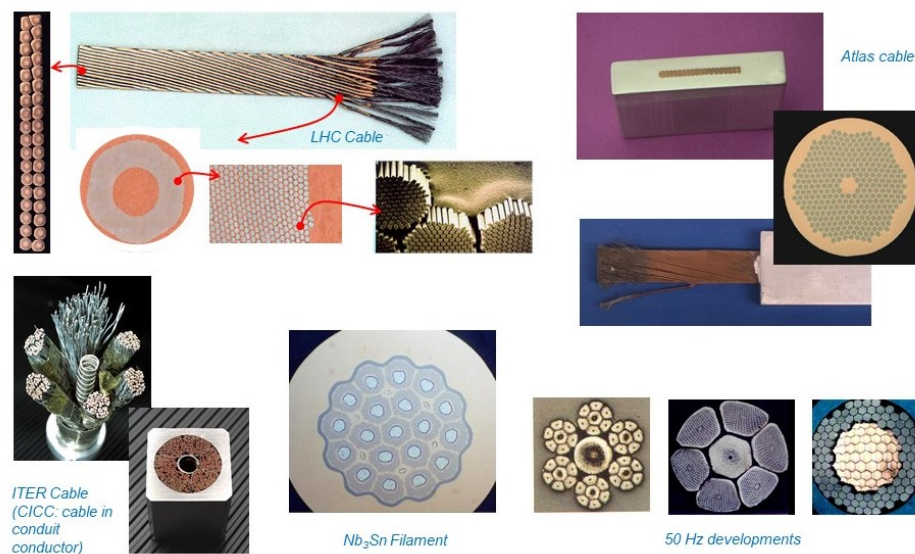


Fig. II.4.17: Examples of cable developments.

II.4.4.1.1 Bean model and wire size influence

In the mixed state, but below the critical current, the superconductor is said “in the critical state”. At equilibrium vortices are perfectly pinned. If one increases the field at the surface, locally the field induces a force that is higher than the pinning force: new vortices enter the material and the vortex front is progressively redistributed. The field inside the superconductor decreases progressively from the surface until it equals to 0, but it is different from the screening current observed in the Meissner state: here the vortex front plays the role of surface current screening. The Bean model proposes that the field decreases

linearly with the slope $-\mu_0 J_C^{\text{Bean}}$, with a constant current density J_C^{Bean} (see Fig. II.4.18, a)). If the slab or wire is large enough, the current density will be much less at its center. This has consequences on the cable design: for a same total section and same applied field, it is more efficient to have many small filaments than one large wire (see Fig. II.4.18, b)). Moreover, large diameters favor instabilities (flux jumps, avalanches instead of progressive penetration of the field).

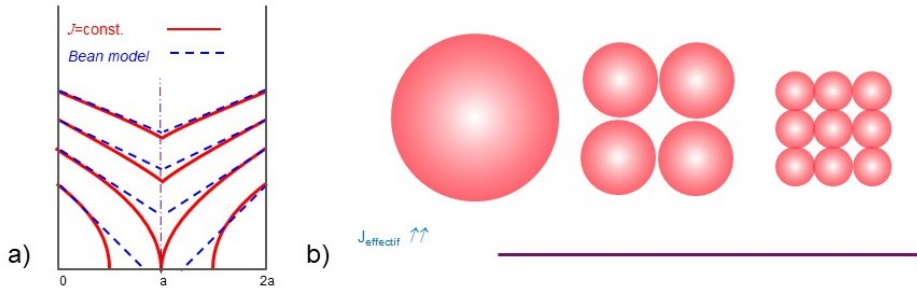


Fig. II.4.18: a) Bean model for the decreasing of the field inside a thin SC slab. b) The effective current density increases if the section of the wire is divided into several filaments

In addition, the filaments must be twisted and transposed. Twisting decouples the wires with respect to the external field while transposing decouples them with respect to their own self-field and prevents non uniform current density to cause a premature quench [13].

II.4.4.1.2 NbTi: compromise between J_C and T_C

For magnet applications, the alloy with composition 46–48% Ti present an optimum for H_{C2} with an acceptable degradation of T_C . Ti has the same atomic radius as Nb, so for this composition, at room temperature, the matrix consists into Nb with a few substitutional Ti (with a T_C that keeps close to the Nb one) along with metallic precipitates of Ti. Upon wire forming (extrusion, wire drawing, intermediate heat treatment) those precipitates are elongated along the drawing (wire) direction and end up in the form of thin flakes with thickness the order of a few nm [14].

As seen in the previous section, best pinning sites are normal, insulating or void regions with dimension $\sim 2\xi$ and parallel to the flux lines. Therefore, those “Ti-flakes” have the perfect dimension and orientation to constitute very effective pinning sites (see Fig. II.4.19, a). The saving in condensation energy is maximum: energy/unit length = $1/2\mu_0 H_{C2} \pi \xi^2 \sim 10^{-11}$ J/m. In DC supercurrent short-circuit the normal areas, but too many pins could result in T_C suppression and current blocking. The exact quantity of pinning centers needs to be adjusted to optimize J_C . On the other hand, those normal conducting precipitates proved very dissipative if submitted to RF, even at very low field [15].

II.4.4.1.3 Nb₃Sn, MgB₂ : brittle material handling

Brittle materials like Nb₃Sn cannot be drawn directly as a wire. Several fabrication processes have been established, where precursor material is first drawn and coiled in place and a thermal treatment allows obtaining the final product (see Fig. II.4.19, b). One main issue is devising an insulating system that can stand the heat treatment. In that case, the critical current is inversely proportional to the grain diameter,

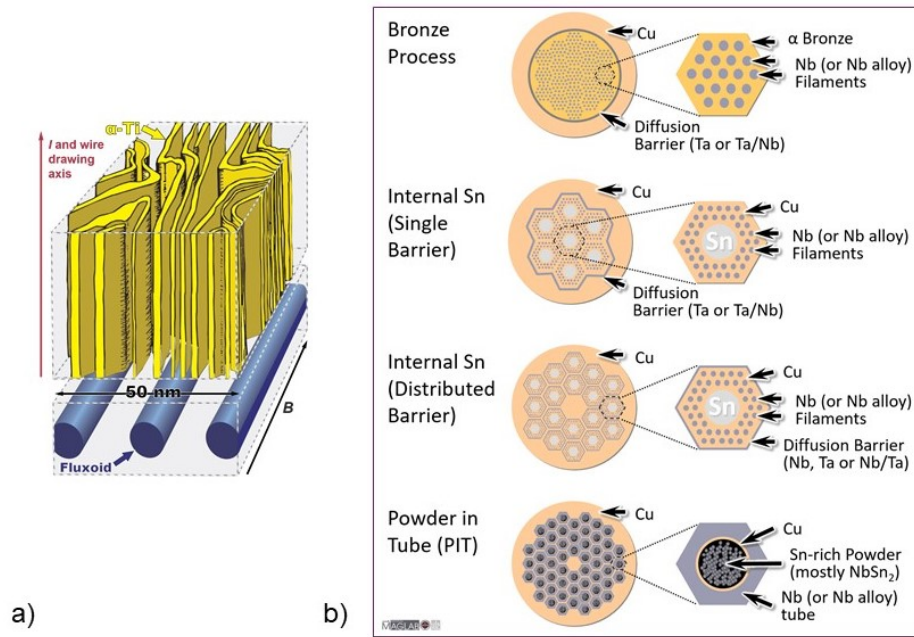


Fig. II.4.19: a) Schematic structure of the Ti “flakes” obtained in a NbTi wire and their comparative size with vortex core (images reproduced with the kind authorization from P.J. Lee, Florida State University). b) Four major designs of commercial Nb₃Sn strands. Reproduced with authorization from the Applied Superconductivity Center Image Gallery, Florida State University [16].

indication that grain boundaries are the main pinning centers. MgB₂ is prepared in a similar way (powder in a tube, drawing and heat treatment).

II.4.4.1.4 HTS: anisotropy, weak links

YBCO family was discovered in the end of the 80s, and very quickly, compounds with T_C above liquid nitrogen were found, auguring a revolution in the use of superconductors, in particular for electric engineering. Unfortunately, this family of material presents two main drawbacks: they are brittle and they are strongly oriented, thus the superconducting properties differ a lot with orientation: J_C is maximum for (a,b) planes and minimum when in the direction parallel to c axis, and $\xi_c \ll \xi_a, \xi_b$ (see Fig. II.4.20). Consequently, a particular orientation needs to be imposed during synthesis. The second drawback is that they are ceramics by nature making them impossible to draw like a conventional metal. It took several decades for consortium including states, research laboratories and companies to be able to develop industrial processes able to produce mostly tapes (only Bi-2212 can be drawn into wire). Cost is still a huge obstacle to the development of industrial applications. The tape shape has its own disadvantages since the demagnetization factor needs to be taken into account, as well as collective effects due to the wiring scheme.

YBCO family members are not conventional superconductors. Cooper pairs are formed but the coupling mechanism is different from the one proposed by BCS. Actually, the coupling mechanism is still not fully elucidated yet. Another difference with conventional superconductors is the symmetry

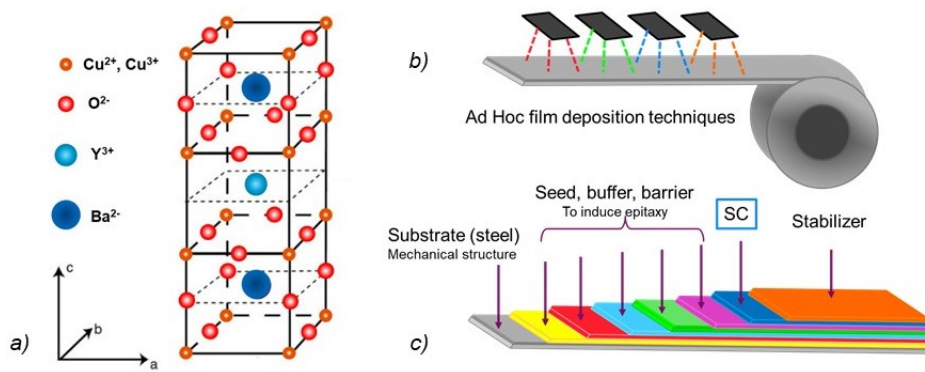


Fig. II.4.20: a) Layered structure of YBCO family. b) Fabrication mode of high T_c tapes: thin films are deposited with several different techniques on a support tape. c) Structure of the final product: the support tape (50–100 μm) plays mainly a mechanical role. Seed, buffer and barrier layers (a few 10s of nm each) aim at obtaining a specific orientation of the superconducting material so that the plane with highest superconducting properties is aligned with the current. The stabiliser is usually copper and/or silver and plays mainly a thermal role.

of the gap (d -wave instead of s wave). This symmetry of the gap implies that they are “directions” where the gap is 0. In RF, the surface resistance dependence is a power-law dependence: $R_S(T) \propto R_i + CT^\alpha$ [17, 18], contrary to BCS behavior where the decrease of R_S is exponential in $-1/T$. At high field, grain boundaries tend to transit in the normal state and are considered as “weak links”. Early penetration of vortex is favored [19]. In RF, some members of this high T_C family exhibit surface resistances one or two orders of magnitude better than copper and current density about one order of magnitude higher, so they are used in the form of thin films for superconducting electronic devices in the 10 GHz–1 THz range, although in the mixed state and in the presence of vortices. At high field (accelerator cavities), the dissipation is still prohibitive [20].

II.4.4.2 RF cavities

As noted in Section II.4.2.2.4, the RF surface resistance is not 0. Nowadays RF cavities are mostly fabricated out of high purity, well-recrystallized, bulk niobium with dedicated surface preparation. Nb is the material with the highest known H_{C1} , so such material is easily maintained in the Meissner state—as required for RF cavities—even in presence of small surface defects.

II.4.4.2.1 Thermal conductivity vs. superconductivity

Bulk niobium is optimized for thermal conductivity rather than superconducting properties, so that small dissipative defects at the inner surface can be thermally stabilized by transporting the heat across the thickness of the cavity wall to the helium bath.

Superconductors are intrinsically bad thermal conductors because many of the conduction electrons that usually transport the heat are now in the form of Cooper pairs. To increase thermal conductivity, one has to decrease the density of electrons scattering centers, which is done by using high purity material with reduced light interstitial elements (H, O, C, N, etc.) concentration. As can be seen in Fig. II.4.21,

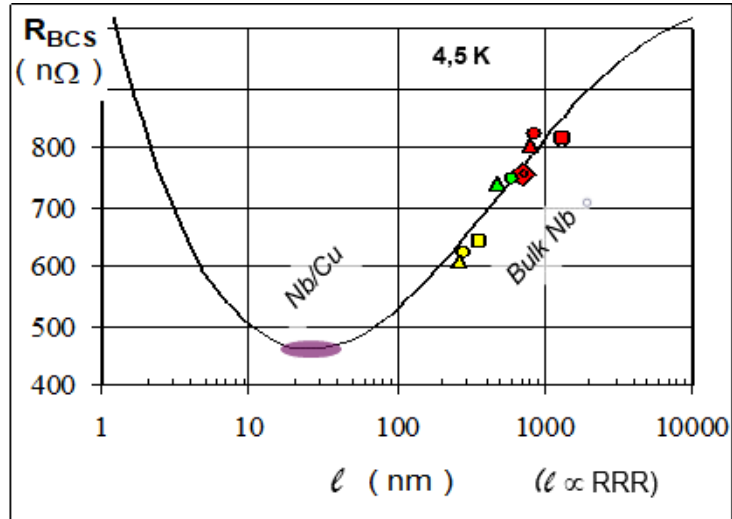


Fig. II.4.21: Surface resistance R_{BCS} vs. mean free path l .

high mean free path materials exhibit a higher RF surface resistance.

II.4.4.2.2 Quasi perfect material on the surface

Because of the electric peak field close to 100 MV/m on the surface, cavities are very sensitive to dust contamination. It has been shown that particles tend to accumulate along electric field lines and form “antennas” that locally enhance the field with a factor β . If β reaches a factor 50 to 500, the local field can surpass 10 GV/m, a field high enough to extract electrons from the surface by tunnel effect. Those electrons are then accelerated by the RF field stored in the cavity, disturb the beam and can provoke heating and X-ray emission when they hit the opposite cavity walls (see Fig. II.4.22).

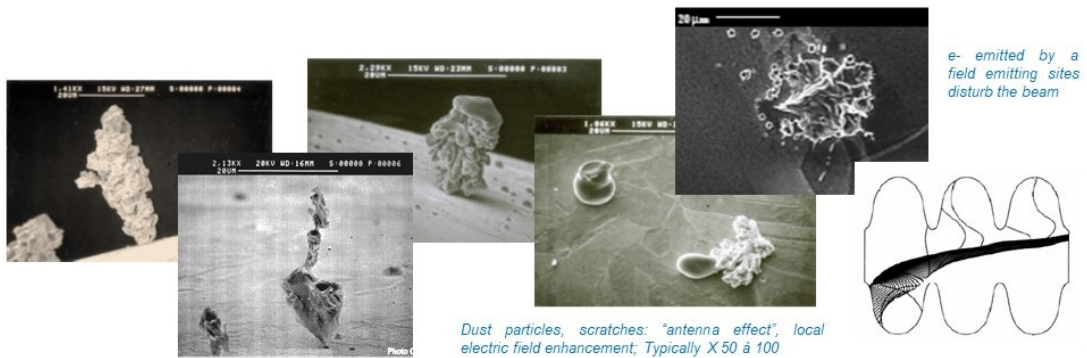


Fig. II.4.22: Example of dust particle accumulation and conductive “antenna” formation. Due to the intense current some of the tips can be processed (melted away), but in some other conditions an electrical breakdown occurs and leaves an immovable emitting site.

One way to prevent this field emission phenomenon is to work in very clean condition, including a high pressure, filtered water rinsing, able to dislodge the smallest dust particles. Cavities are assembled inside clean rooms with the same cleanliness level as used in microelectronics.

II.4.4.2.3 Quasi-perfect material under the surface

When one switch from copper where skin depth is the order of a few micron to niobium, where the field penetration depth is about 40 nm, the quality of the surface becomes preponderant. The damage layer due to contact with tooling during the fabrication phases (rolling equipment to prepare Nb sheets, deep drawing dyes, thermal strain during welding, etc.) are all liable to leave crystalline defects and affect superconductivity (Fig. II.4.23). Therefore, the damaged surface (typically 150–200 μm) needs to be polished away. It is usually done either by electropolishing (EP) or by buffered chemical polishing (BCP) which is in fact more an etching process than real polishing and produces some roughness. Recrystallization treatment (800°C, 2 h or 650°C, 8–10 h) is also mandatory. Not only it improves the crystalline quality of the surface, but it also reduces the density of nucleating sites for niobium hydrides on the surface. Those hydrides NbH_x form pyramidal crystals on the surface and exhibit degraded superconducting properties. So they provide early entry points for vortices and trigger early quenches on untreated cavities [6].

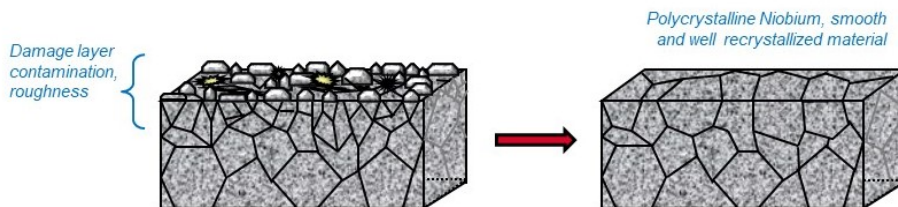


Fig. II.4.23: Representation of the damage layer: crystallites in contact with tools are deformed, accumulating high density of crystalline defects (see Section II.4.3.4.1). Not only superconducting properties are affected, but also the risk of poorly expelling flux lines during cooling is increased.

II.4.4.2.4 Improving surface resistance without affecting thermal conductivity

With various heat treatments, it is possible to affect the surface composition and the distribution of light elements on a thickness ranging from 10 nm to a few penetration depths of the material. Since only the surface is affected, it is a way to monitor the surface superconductivity without affecting the thermal conductivity of the bulk of the cavity wall. Very high Q_0 with a somewhat limited E_{acc} can be reached by nitrogen or oxygen doping (see Fig. II.4.24). The various recipes [21] result in a flat distribution of some 100 ppm N inside Nb over several 100 nm depth. The mechanism of the decrease of the surface resistance with field is still debated, but there are some indications that the surface T_C is affected by the presence of a large quantity of interstitials, which could explain why the accelerating field is limited. More recently it was discovered that medium T -baking around 300–400 °C [22, 23], with no nitrogen, was producing the same type of behavior. In this case, oxygen from the oxide layer diffuses from the surface and occupies the same interstitial spaces as nitrogen. Both N and O are known to affect the diffusion rate of H inside Nb⁹, and as shown in Fig. II.4.21, the surface resistance is minimum for a mean free path about 10 nm. More complex mechanisms need to be implemented to fully explain the observed behavior [21].

⁹H moves relatively freely inside Nb at room temperature, but due to elastic interactions with defects, in particular the oxide–metal interface, surface segregation is observed (see Section 3.4.3).

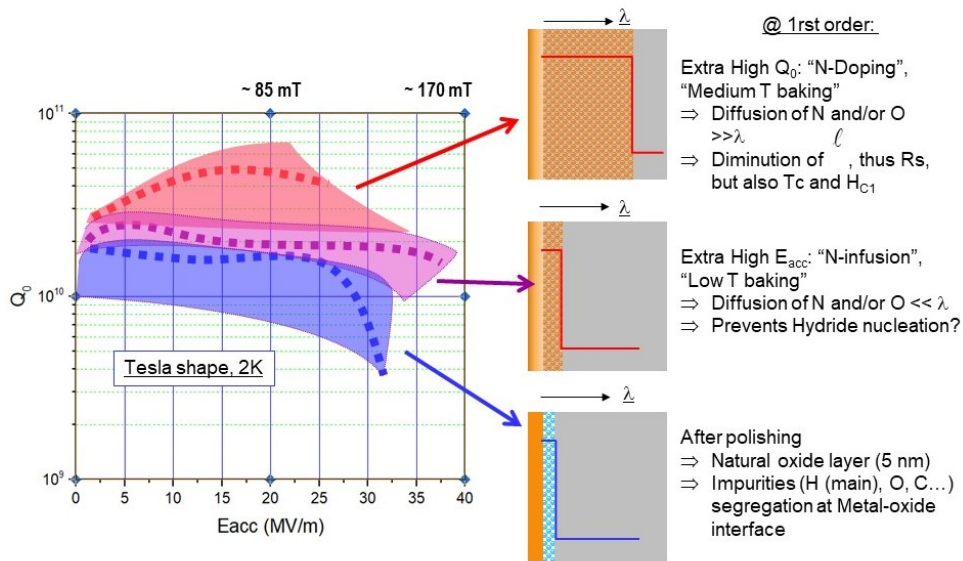


Fig. II.4.24: Schematic behavior of cavities after various surface preparation recipes.

Lower temperature treatments (120°C, 48 h, with or without nitrogen) also affect the behavior of cavities, enhancing the accelerating field, without necessarily increasing the Q_0 . The profile of impurities keeps concentrated in the first 10 nm of the surface. Knowing that hydrides are very good candidates to early vortex penetration, the main effect seems to be the prevention of large hydrides precipitates. The important result is that one can monitor the behavior of the cavities to their applications, without changing the overall bulk Nb technology. High Q_0 are required for high duty cycle and CW machines, while high E_{acc} rather apply to longer machines such as colliders.

II.4.4.2.5 Future: thin film cavities

Bulk Nb is a rather expensive technology, so very early the possibility to deposit thin film of Nb inside a copper cavity has been explored. Unfortunately, the crystalline quality of thin film is far lower than that of bulk cavity. During more than 50 years an active R&D has been conducted without real improvement, and this technology has been confined to circular machines where the accelerating field is not paramount. Only recently, by combining better surface preparation of copper cavities with higher density deposition techniques the quality of Nb thin films could be improved. High T_C material like NbN, Nb₃Sn or MgB₂ have also been explored. Here again, these materials, which exhibit very small ξ compared to Nb have shown to be very sensitive to surface defects. The challenge for the near future is to achieve deposition onto copper cavities and reaching an operating temperature of 4.5 K instead of 2 K. The simplification of cryogenic installation and consumption decrease is expected to reduce investments as well as operating costs. Today active R&D exists in this domain, but no cavity production has been completed. Nb₃Sn layers prepared by Tin thermal diffusion inside bulk Nb cavities show the same performances at 4.5 K as bulk Nb at low K but are limited in accelerating field around 25 MV/m (~ 100 mT) whereas record cavities reach 50 MV/m (210 mT) [24].

As explained before, the main difficulty is to maintain the superheating state in the presence of

defects. In 2006, multilayer structures were proposed to overcome this difficulty [25]. By inserting a dielectric layer (transparent to RF) a few 100 nm under the surface, one can block the avalanche penetration of vortices. The initial vortex loop converts into a small portion of vortex plus a small portion of antivortex that readily coalesce after a few RF periods (see Fig. II.4.25).

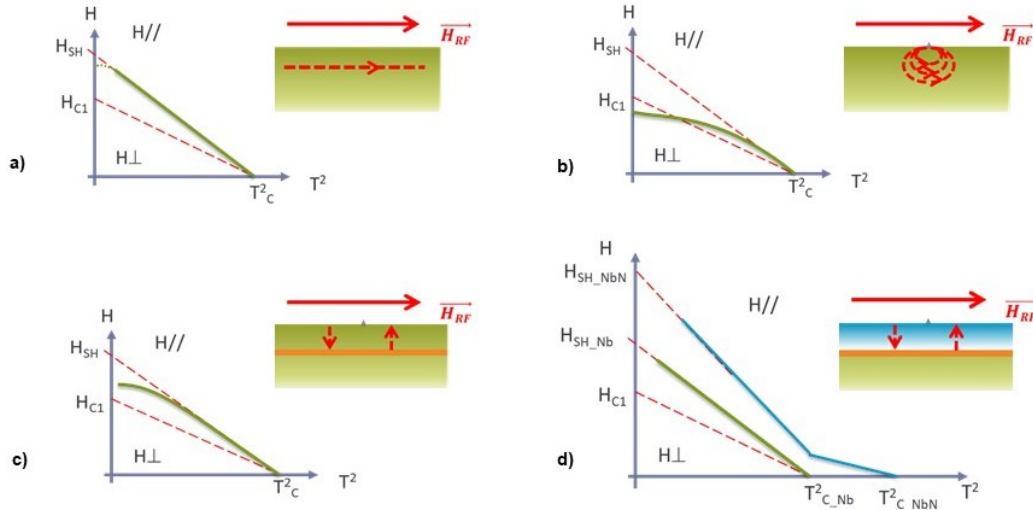


Fig. II.4.25: Principle of multilayer. a) In the ideal case, Bean–Livingston barrier stabilizes the superheated state and Meissner state can be maintained above H_{C1} . b) In the presence of a surface defect, vortex loops can enter the SC and at high field the dissipation are too high to maintain the superheated state. c) In the presence of a dielectric layer, the initial vortex loop converts into a small portion of vortex plus a small portion of antivortex that readily coalesce after a few RF periods, preventing local heating and avalanche penetration. The use of a high T_C superconductors with thickness $\leq \lambda_L$ allows to access high accelerating field with decreased surface resistance.

Moreover, if one uses a higher T_C SC with thickness $\sim \lambda_L$ as a top layer, then its H_{C1} is artificially increased, allowing enhancing the RF field inside the cavity. The BCS surface resistance of a higher T_C material is expected to be smaller, so overall performances of a coated cavity is expected to be improved in accelerating field as well as in quality factor. These structures have been explored with magnetron sputtered material, showing that the multilayer structure is much less sensitive to defects [26].

II.4.5 Conclusion

Nowadays one can notice that most advanced technologies (materials for fusion, nuclear power, fuel cells, solar cells, batteries, etc., and accelerators) are limited by material issues. Even if the technology is well mastered at the lab level, one will be facing reproducibility issues, the need to reduce costs, and finding solutions to aging problems, when switching to production level. It is particularly true when a technology is pushed to its ultimate limits as in the case of accelerators:

- Most of the time the choice of the material results from a compromise between multiples constraints: mechanical, thermal, stability, superconductivity, costs, etc., and interdisciplinary work is mandatory: multiple and complementary expertise is necessary;

- Meeting experts outside the accelerators community is often a way to prevent costly and long R&D steps, as the answer sometimes already exists elsewhere (do not re-invent the wheel!);
- Be also prepared to meet diagnostics issues: where does the breakdown come from when many conjugate factors occur together? A large part of the work consists into developing diagnostics systems;
- Finally, allow yourself to break traditions (but not too often—it costs money).

References

- [1] Y. Cao *et al.*, Unconventional superconductivity in magic-angle graphene superlattices, *Nature* **556** (2018) 43–50, [doi:10.1038/nature26160](https://doi.org/10.1038/nature26160).
- [2] D. Mattis and J. Bardeen, Theory of the anomalous skin effect in normal and superconducting metals, *Phys. Rev.* **111** (1958) 412, [doi:10.1103/PhysRev.111.412](https://doi.org/10.1103/PhysRev.111.412).
- [3] A. Gurevich, Multiscale mechanisms of SRF breakdown, *Phys. C* **441** (2006) 38–43, [doi:10.1016/j.physc.2006.03.024](https://doi.org/10.1016/j.physc.2006.03.024).
- [4] R. Prozorov and V.G. Kogan, Effective demagnetizing factors of diamagnetic samples of various shapes, *Phys. Rev. Appl.* **10** (2018) 014030, [doi:10.1103/PhysRevApplied.10.014030](https://doi.org/10.1103/PhysRevApplied.10.014030).
- [5] C. Bean and J. Livingston, Surface barrier in type-II superconductors, *Phys. Rev. Lett.* **12** (1964) 14–16, [doi:10.1103/PhysRevLett.12.14](https://doi.org/10.1103/PhysRevLett.12.14).
- [6] C.Z. Antoine, Materials and surface aspects in the development of SRF niobium cavities, *EuCARD Ed. Ser. Accel. Sci. Technol.* **12** (2012) EuCARD-BOO-2012-001, <https://inspirehep.net/literature/1186049>.
- [7] J. Vestgård *et al.*, Lightning in superconductors, *Sci. Rep.* **2** (2012) 886, [doi:10.1038/srep00886](https://doi.org/10.1038/srep00886).
- [8] T. Matsushita, *Flux pinning in superconductors*, 2nd ed. (Springer Berlin, 2014), [doi:10.1007/978-3-642-45312-0](https://doi.org/10.1007/978-3-642-45312-0).
- [9] H. Ullmaier *et al.*, Pinning of flux lines in superconducting niobium due to point defects, *Phys. Stat. Sol. B* **41** (1970) 671–679, [doi:10.1002/pssb.19700410222](https://doi.org/10.1002/pssb.19700410222).
- [10] C.Z. Antoine, Influence of crystalline structure on RF dissipation in superconducting niobium, *Phys. Rev. Accel. Beams* **22** (2019) 034801, [doi:10.1103/PhysRevAccelBeams.22.034801](https://doi.org/10.1103/PhysRevAccelBeams.22.034801).
- [11] A. Pautrat *et al.*, Electrodynamics of the vortex lattice in untwinned YBaCuO by complex impedance measurements, *Eur. Phys. J. B* **33** (2003) 279–284, [doi:10.1140/epjb/e2003-00167-6](https://doi.org/10.1140/epjb/e2003-00167-6).
- [12] G. Ciovati and A. Gurevich, Evidence of high-field radio-frequency hot spots due to trapped vortices in niobium cavities, *Phys. Rev. Accel. Beams* (2008) **11** 122001, [doi:10.1103/PhysRevSTAB.11.122001](https://doi.org/10.1103/PhysRevSTAB.11.122001).
- [13] M.N. Wilson, Practical superconductors for accelerators cable, Proc. CERN Accelerator School on Superconductivity and Cryogenics for Accelerators and Detectors, Erice, Italy, 8–17 May 2002, Eds. S. Russenschuck and G. Vandoni, CERN-2004-008, pp. 58–70, [doi:10.5170/CERN-2004-008.58](https://doi.org/10.5170/CERN-2004-008.58).

- [14] P.J. Lee, and D.C. Larbalestier, Niobium-titanium superconducting wires: Nanostructures by extrusion and wire drawing, *Wire J. Int.* **36:2** (2003) 61–66, [CiteSeerX](#) Slightly edited (no APC and cabling sections) and monochromatic form.
- [15] N. Bazin *et al.*, Study of NbTi welded parts" Proc. 16th Int. Conf. on RF Superconductivity, Paris, France, 23–27 Sep. 2013, Eds. C. Antoine, S. Bousson and G. Martinet (JACoW, Geneva, 2014), pp.659–662, <https://accelconf.web.cern.ch/srf2013/papers/tup085.pdf>.
- [16] National High Magnetic Field Laboratory, Nb₃Sn image gallery (National MagLab, Tallahassee, FL), last accessed 17 Nov. 2023, <https://nationalmaglab.org/magnet-development/applied-superconductivity-center/image-gallery/nb3sn-image-gallery/>.
- [17] A. Gurevich and G. Ciovati, Dynamics of vortex penetration, jumpwise instabilities, and nonlinear surface resistance of type-II superconductors in strong RF fields, *Phys. Rev. B* **77** (2008) 104501, [doi:10.1103/PhysRevB.77.104501](https://doi.org/10.1103/PhysRevB.77.104501).
- [18] J. Mao *et al.*, Consequences of d-wave superconductivity for high frequency applications of cuprate superconductors, *IEEE Trans. Appl. Supercond.* **5** (1995) 1997–2000, <https://doi.org/10.1109/77.402978>.
- [19] A. Gurevich, To use or not to use cool superconductors?, *Nature Mater.* **10** (2011) 255–259, [doi:10.1038/nmat2991](https://doi.org/10.1038/nmat2991).
- [20] E. Hannachi and Y. Slimani, RF and microwave applications of high temperature superconductors, in *Superconducting materials: Fundamentals, synthesis and applications* (Springer, Singapore, 2022), pp. 373–399, https://doi.org/10.1007/978-981-19-1211-5_13.
- [21] P. Dhakal, Nitrogen doping and infusion in SRF cavities: A review, *Phys. Open* **5** (2020) 100034, [doi:10.1016/j.physo.2020.100034](https://doi.org/10.1016/j.physo.2020.100034).
- [22] H. Ito *et al.*, Influence of furnace baking on Q–E behavior of superconducting accelerating cavities, *Prog. Theor. Exp. Phys.* **2021** (2021) 071G01, [doi:10.1093/ptep/ptab056](https://doi.org/10.1093/ptep/ptab056).
- [23] S. Posen *et al.*, Ultralow surface resistance via vacuum heat treatment of superconducting radio-frequency cavities, *Phys. Rev. Appl.* **13** (2020) 014024, [doi:10.1103/PhysRevApplied.13.014024](https://doi.org/10.1103/PhysRevApplied.13.014024).
- [24] U. Pudasaini *et al.*, Nb₃Sn films for SRF cavities: genesis and RF properties, Proc. 19th Int. Conf. on RF Superconductivity, SRF2019, Dresden, Germany, June 30–July 5, 2019, Eds. V. Schaa, P. Michel and A. Arnold (JACoW, Geneva, 2019), pp. 810–817, [doi:10.18429/JACoW-SRF2019-THFUA6](https://doi.org/10.18429/JACoW-SRF2019-THFUA6).
- [25] A. Gurevich, Enhancement of RF breakdown field of SC by multilayer coating, *Appl. Phys. Lett.* **88** (2006) 88 012511, [doi:10.1063/1.2162264](https://doi.org/10.1063/1.2162264).
- [26] C.Z. Antoine *et al.*, Optimization of tailored multilayer superconductors for RF application and protection against premature vortex penetration, *Supercond. Sci. Technol.* **32** (2019) 085005, [doi:10.1088/1361-6668/ab1bf1](https://doi.org/10.1088/1361-6668/ab1bf1).